



Delamination damage imaging method of CFRP composite laminate plates based on the sensitive guided wave mode

Hui Zhang, Jing Sun, Xiaobo Rui^{*}, Si Liu

State Key Laboratory of Precision Measuring Technology and Instruments, Tianjin University, Tianjin 300072, China



ARTICLE INFO

Keywords:
CFRP composite laminate
Delamination damage
Wavenumber
Finite element simulation

ABSTRACT

This research is related to a detection and imaging method of delamination damage in CFRP composite laminate structures. Conventional guided wave detection methods often use the reflected wave signal at the defect as an indicator. However, the reflected wave signal caused by delamination damage is very weak compared with surface damage such as depressions, which brings great difficulty to delamination detection. The aim is to demonstrate a method for detecting delamination damage such that estimation of the morphology of the delamination can be obtained. This method uses full-wavefield data and is based on incident waves rather than reflected waves. This method weakens the original A0 mode through annular band-stop filtering, and at the same time enhances the sensitive modes in the full wavefield data. The intensity of enhanced signal in the time domain is used to image the delamination. The simulation model is used for modeling of guided waves propagation and interaction with delamination damage in CFRP composite laminate. The method is first illustrated on simulated data, and then tested on experimental results. It is shown that it is possible to visualize the delamination damage morphology by using the proposed SME imaging method.

1. Introduction

Carbon fiber reinforced polymers (CFRP) composite laminate plate is widely used in aircraft structure for their excellent quality in strength, stiffness, high-temperature resistance, and light weight. Delamination tends to occur due to the stresses in the lamina principal directions varying from lamina to lamina [1]. It can be caused by sources like manufacturing defects, impact events, compression, and fatigue. Among them, impact is a primary source of delamination. Composite materials and metallic materials react differently when impacted. When a CFRP composite component is impacted at low energy levels, it may not show any visible sign of external damage while at the same time receiving nonvisible internal damage, such as delamination [2]. When subjected to unexpected impact during regular operation, such as impact due to hail, metallic-built components show visible signs such as dents. These materials can still be used without presenting a risk of failure. But in composite materials, the barely visible impact damage has been shown to reduce the residual compressive strength in the area affected by impact damage. The impact force results in the crushing of both, the fibers as well as the resin in the impacted area, while at the same time the deflected laminate triggers interlaminar shear failures resulting in

delamination. Therefore, the residual compression strength as well as the tensile strength of the composite laminate, are reduced [3]. The nonvisible delamination is more difficult to detect than other visible interlaminar fractures, especially for the small range of delamination defects. Therefore, an accurate nondestructive testing method needs to investigate delamination damage.

Many non-destructive testing (NDT) techniques are used in the process of composite materials testing such as ultrasonic testing [4–6], X-rays [7,8], eddy current testing [9,10], active thermography [11,12], etc. And each method has its advantages and limitations such as radiation pollution, high cost, limited detection objects, uncertain sensitivity, and so on. Among them, ultrasonic testing has high sensitivity, fast speed, low cost, is harmless to the human body, and can locate and quantify defects. Therefore, ultrasonic testing can be used for delamination detection as a means of NDT.

Ultrasonic C-scan is sensitive to internal defects and can identify delamination through transmitted waves or reflected echoes, but immersion testing system limits its application scenarios [13]. Air-coupled ultrasonic C-scan overcomes the above difficulty, but the severe attenuation in the air guides to a lower frequency signal, which causes its sensitivity to depend on the scanning step distance [14,15]. Phased

* Corresponding author.

E-mail address: ruixiaobo@tju.edu.cn (X. Rui).

array ultrasonic testing costs less time, but the sensitivity becomes worse as the distance from the sensor is farther [16,17]. Compared with the transmitted waves or reflected waves, guided waves are more suitable for detecting plate structures. Guided waves are less attenuated in the plate and more sensitive to internal delamination damage [18–20].

The guided wave contains a lot of information about the structure and the damage within the plate. Some studies focus on the characteristics of wave propagation, which mainly include the time of flight (TOF), wave mode conversion, wave scattering, attenuation, et al. [21–24]. K. Balasubramaniam obtained the probability of debonding from the signal amplitude on the path [25]. H. Mei et al. used the normal wedge to excite a single-mode guided wave, and compared the signal amplitude of the damaged area and the non-destructive area [19]. B. Williams and Xiaofeng Liu use the relative intensity of nonlinear second harmonic as damage index for positioning imaging [26,27]. C.S.Rekatasinas et al. detected delamination defects using modal transformation [24,28]. These methods often require clear wave packets, which are difficult to obtain due to the complex modes, reflection, and scattering waves.

To separate the aliased wave packets and modes, Fourier transform is performed to the original wavefield data [29]. In the frequency-wavenumber-domain, the modal change information caused by delamination on Lamb waves can be easily distinguished, which is difficult to achieve with time-domain information [30,31]. Nitesh P. Yelva et al. used the nonlinear effect of the guided wave at stratification to obtain damage information from the spectrum of the fundamental wave and high order harmonic wave and defined the spectrum damage index (SDI) to measure the size of damage [32]. Hanfei Mei has studied the mode conversion caused by delamination [33]. Paweł Kudela et al. used the wavefield characteristics of Lamb waves to detect and evaluate cracks in plate-like structures [34,35]. However, there is a big difference between delamination damage and depression damage, that is, when the guided wave propagates to the crack damage, a strong reflected wave will appear, but the delamination damage has a small projection perpendicular to the wave propagation direction, so the reflection is not obvious. The main energy and information of Lamb waves lie in direct waves, and the characteristics of the incident waves should be paid more attention to. In summary, although a series of studies have been carried out about the delamination in composite materials, there are still non-negligible measurement errors due to the weak delamination signals.

In response to the above problems, we studied the interaction between delamination and guided waves by numerical simulation. The aim is to investigate the guided wave behavior in the presence of delamination damage to propose a delamination detection method. This paper proposes a delamination damage sensitive mode enhancement (SME) imaging method using incident wavefield. It processes the wavefield signals in the wavenumber domain and avoids processing aliased waveform signals in the time domain. The SME method set up an elliptical ring filter to attenuate the original mode and enhance the sensitive-to-delamination mode in the plate. Finally, image the delamination with the enhanced sensitive mode.

This paper is organized as follows. Section 2 gives the CFRP composite laminate plate models of this research. And also studied the effect of delamination on guided waves. Section 3 describes the detailed steps of the SME imaging method. In Section 4, the results of the SME imaging method acting on simulations and experiments. Section 5 concludes the paper with novelties and discussions.

2. CFRP composite laminate plate models with delamination damage

2.1. Details of material properties

In this research, the CFRP composite laminate plate consists of 16 layers with fiber orientation [+45/-45/0/0]_S shown in Fig. 1, which total thickness of the specimen is 2 mm. The material properties for

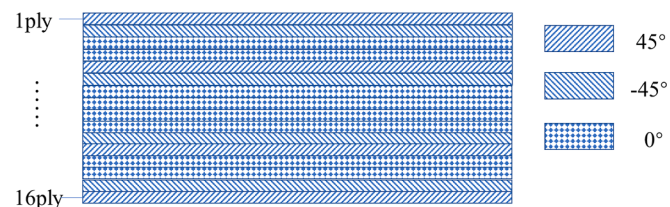


Fig. 1. Layer direction.

single layer were provided by the manufacturer istar-space. The characteristic parameter table of the CFRP board in this article is shown in Table 1.

Guided waves are elastic wave in the plate structure, which have multiple modes, and its propagation in the plate is complicated. The mode of the guided wave in the plate can be obtained by the dispersion curve. The wave propagation in the composite material is very complicated, due to its heterogeneity, anisotropy, and multi-layer structure. In addition, the wave mode speed depends on the layer and layer division, wave propagation direction, frequency, and interface conditions. Multi-layer composite laminates dispersion curves can be obtained by applying the transfer matrix method or the global matrix method to the single-layer board dispersion equation (Fig. 2).

2.2. Finite element simulations setting

Using the COMOSL software, the finite element method (FEM) is carried out to simulate the propagation of guided waves in the CFRP composite laminate plate.

The overall schematic diagram of the specimen is shown in Fig. 3, and there are 5 specimen models with different damages simulated for comparison. The center of the specimen is located at the origin of the Cartesian coordinate system, and the center of the damage is located at (50,0) mm in the x-y plane. Three of the damage are invisible delamination inside the plane, one of them is an exposed depression, and the last specimen is undamaged. The through-thickness locations of delamination damages are arbitrarily set on the top side of plate since the ply direction of the laminate is symmetrical. The details of the damage are shown in Table 2. Delamination is modeled by subtracting a thin cuboid from the original cuboid board by Boolean operation. The size of the thin cuboid is 20 mm × 20 mm × 0.1 mm, and obviously, the thickness of this layer is 0.1 mm.

The excitation signal was applied to the center of the upper surface at the plate and the expression is as Eq. (1)

$$u(t) = v_{pp} \left[H(t) - H\left(t - \frac{N}{f_c}\right) \right] \times \left(1 - \cos \frac{2\pi f_c t}{N} \right) \sin 2\pi f_c t \quad (1)$$

where $H(t)$ is Heaviside step function, f_c is the excitation frequency, and N is the number of peaks. In Fig. 4, the excitation signal in time-domain is presented. In this paper, the excitation frequency is selected as 200 kHz and the number of peaks is set to 5. It can be seen from the dispersion curve in Fig. 2 that the lower the frequency, the fewer modes exist in the board. When the excitation frequency is lower than 400 kHz, only two modes, A0 and S0, exist. The frequency selection is a compromise between damage sensitivity and wave attenuation (low-frequency waves are less sensitive to damage whereas high-frequency waves attenuate very fast due to damping properties of composite laminate).

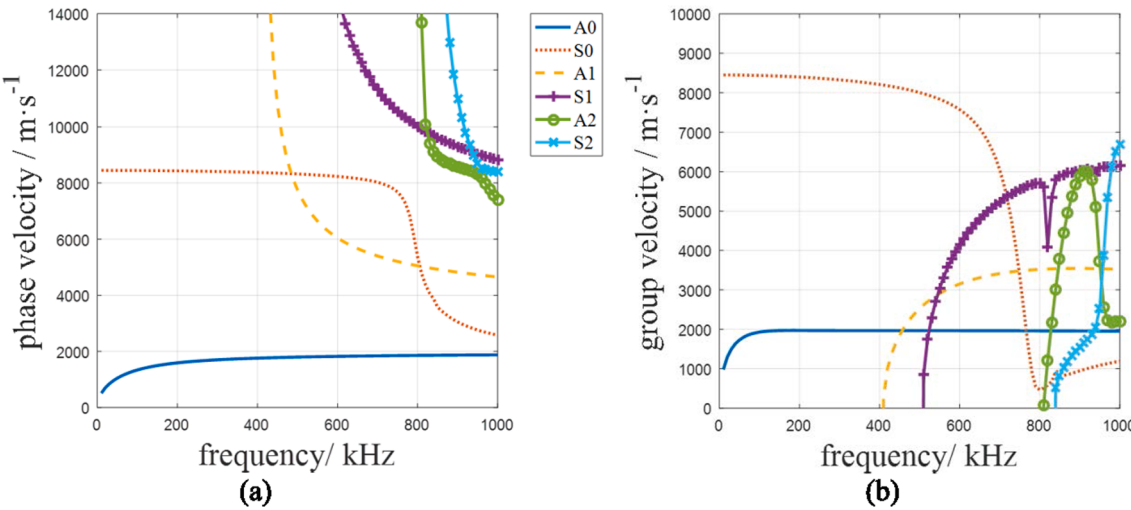
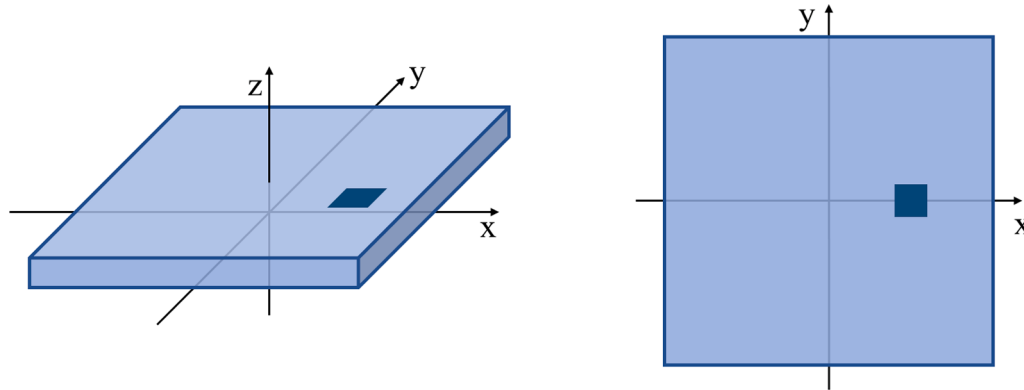
2.3. Guided waves propagation law in the CFRP composite plate with delamination damage

Incident guided waves contain two modes according to dispersion curves, and due to A0 mode being dominated by out-of-plane (transverse) displacements whereas S0 mode is dominated by in-plane

Table 1

Material parameters of a single layer of CFRP plate.

ρ (kg/m ³)	E ₁ (GPa)	E ₂ (GPa)	E ₃ (GPa)	G ₁₂ (GPa)	G ₁₃ (GPa)	G ₂₃ (GPa)	ν_{12}	ν_{13}	ν_{23}
1600	172	11.6	11.6	7.8	7.8	3.9	0.36	0.36	0.55

**Fig. 2.** 16plies CFRP composite laminate plate dispersion curves in 0°: (a)phase velocity, (b)group velocity.**Fig. 3.** Specimen models.

displacements, the signal of A0 mode is stronger than S0 when observed from the out-of-plane displacement. In the original plate, the forward traveling and reflection waves of the A0 mode can be observed as shown in Fig. 5.

A few points along the y-axis were selected and shown in Fig. 6. The group velocity of the wave packet can be calculated with the wave crest, and it's 1482 m/s. According to the theoretical dispersion curves, this wave packet matches the A0 mode.

As for a plate structure with damage, the forward traveling A0 mode was affected by the delamination or depression, the wavefield in each plate is shown in Fig. 7. The points located at (50, 0) mm in four plates vibrated as Fig. 8.

Three significant features were found in the time-domain signal from simulations results. The first one is that the reflected wave signal caused by delamination is smaller than that caused by cracks or surface damage. Fig. 7 (b) shows the wavefield at 50 μ s in each plate. It is clear that the depression led to an obvious reflection at the edge of the damage, but the delamination didn't. The projection perpendicular to the direction of wave propagation of the delamination is smaller than depressions and it has less ability to cause reflected waves. Therefore, most energies of the

Lamb wave keeps on spreading through the delamination.

The second one is that delamination damage can trap energy in the damaged area. Fig. 8 shows the center point (50, 0) mm only vibrated one A0 wave packet in an original CFRP composite laminate plate and vibrated sustained after the A0 wave packet in the delaminated plate. Some of the crests after the first wave packet are even higher than the original A0 peak. As for the depression damage, the vibration disappeared earlier than the delamination damage. It means that the delamination trapped energy in its area, and depression damage doesn't have such characteristics. This phenomenon means that energy may be used for delamination detection. However, the waves after the A0 wave packet are so overlapped that it is difficult to analyze in the time-domain. This signal is more suitable for processing in the frequency-wavenumber domain.

The third one is that the original Lamb waves are divided into the top and bottom plates by the delamination. The top waves and the bottom waves propagate separately and affect each other at the same time. When observed from the top surface of the plate, Lamb waves properties in the top plate can be obtained. Therefore, the sensitive mode exists in the top plate, and be affected by the delamination location.

Table 2
Details of damage in each specimen.

	Damage type	Position in thickness	Damage section diagram	size
Plate1	Invisible delamination	Between 2ed ply and 3rd ply		$d = 20 \text{ mm}$
Plate2	Invisible delamination	Between 4th ply and 5th ply		$d = 20 \text{ mm}$
Plate3	Invisible delamination	Between 6th ply and 7th ply		$d = 20 \text{ mm}$
Plate4	Surface damage	Between 8th ply and 9th ply		$d = 20 \text{ mm}$
Plate5	Undamaged	Non		

3. Sensitive mode enhancement imaging method

In order to make full use of the laws summarized in subsection 2.3, this research proposed a sensitive mode enhancement (SME) imaging method. This method processes the full wavefield data through an elliptic ring filter in the frequency-wavenumber-domain. It weakens the original A0 mode through annular band-stop filtering and enhances the mode component sensitive to delamination, and images the

delamination area utilizing its energy signal. This method involved full wavefield data in the calculation, which contains more information compared with a single wave packet or individual reflect wave. The flow diagram of the method is shown in Fig. 9.

- (1) Transform time-domain wavefield information to frequency domain through Fourier transform.

When studying the propagation of waves in a spatial domain, perform three-dimensional Fourier transform as Eq. (2) on wavefield data $w(x,y,f)$ to wavenumber-domain $W(k_x,k_y,f)$:

$$W(k_x, k_y, f) = \int_{-\infty}^{+\infty} \int_{-\infty}^{+\infty} \int_{-\infty}^{+\infty} w(x, y, t) e^{-j(k_x x + k_y y + ft)} dx dy dt, \quad (2)$$

where $w(x,y,f)$ is the out-of-plane displacement, and $W(k_x, k_y, f)$ is the wavefield data in the wavenumber-domain.

- (2) Design the filter mask.

Using the semi-analytical finite element (SAFE[36]) method, the dispersion curve calculations are performed for composite plates made of 1 single ply, 2 plies, and so on up to the total plate thickness (with each ply increment corresponding to the plate layup) in all directions. The 2D wavenumber in the orthogonal direction can be obtained by decomposing the wavenumber in each direction by the Eq. (3). And the dots can be approximated as an ellipse. Taking 0° as an example, the value of the A0 modal wave at 200 kHz is 0.7892 rad/mm. Since the frequency spectrum has a certain width, a band rejection filter with a bandwidth of $0.65 \sim 0.95$ rad/mm can be designed. According to this method, a two-dimensional A0 mode filter mask $M_f(k_x, k_y, f)$ can be

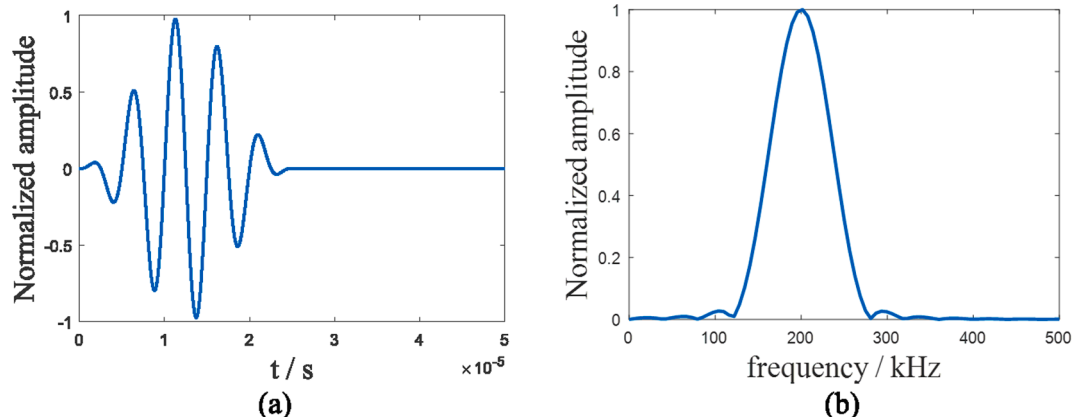


Fig. 4. Excitation signal in (a) time-domain and (b) frequency-domain.

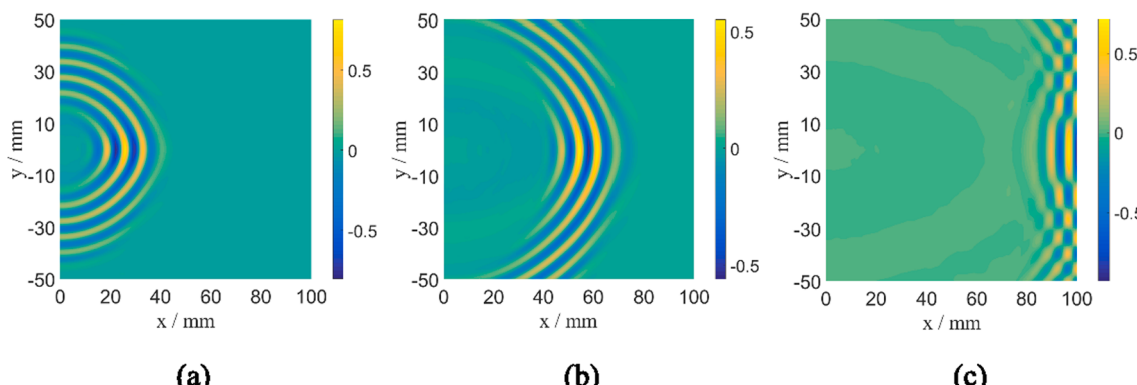


Fig. 5. Out-of-plane displacement of guided waves in plate 4 at (a) 30 μs ; (b) 50 μs ; (c) 80 μs in plate 5.

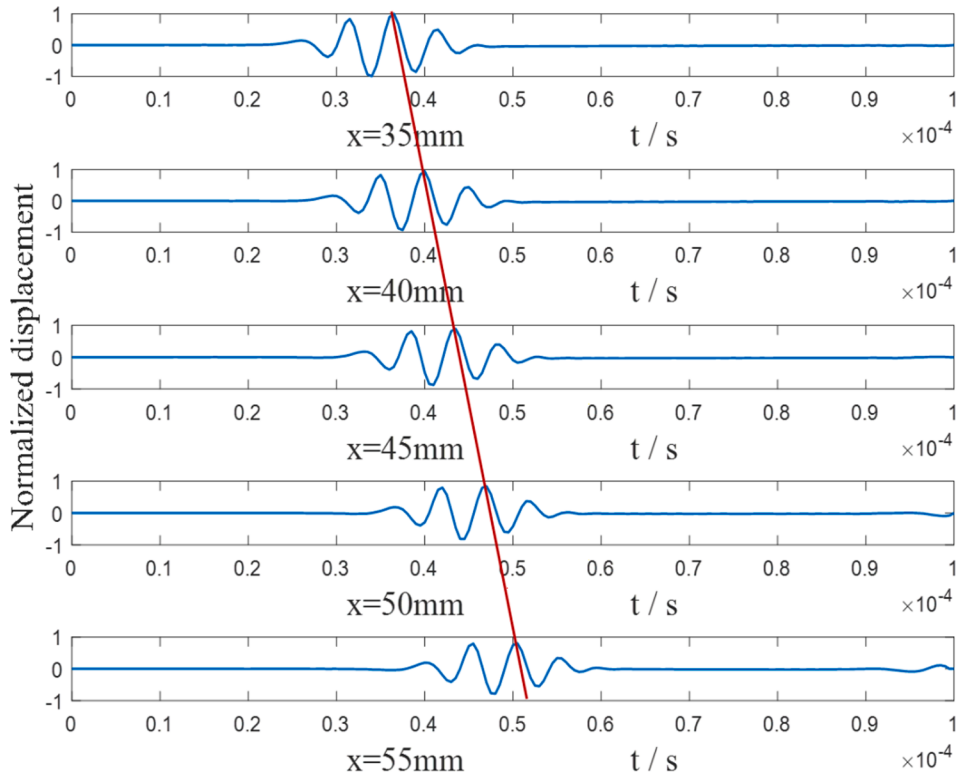


Fig. 6. Normalized displacement of a few points in plate 5.

designed as the Eq. (4).

$$\begin{aligned} k_x &= k_\theta \cdot \cos\theta \\ k_y &= k_\theta \cdot \sin\theta \end{aligned} \quad (3)$$

Where θ is the included angle between the 0° fiber and the wave propagate direction.

(3) Enhance the sensitive mode component.

Multiply the wavefield data in the wavenumber-domain $W(k_x, k_y, f)$ with the filter $M_f(k_x, k_y)$ as Eq. (5). This step removes the original A0 mode and enhances the other modes at the same time. As the frequency selection is directly related to the wave value, the frequency selection

$$M_f(k_x, k_y, f) = \begin{cases} 1 & |k| \frac{k_{0\min}^2}{k_{\frac{\pi}{2}\min}} \left(1 - \frac{\sqrt{k_{\frac{\pi}{2}\min}^2 - k_{0\min}^2}}{k_{\frac{\pi}{2}\min}} \cos\theta \right) \\ 0 & \frac{k_{0\min}^2}{k_{\frac{\pi}{2}\min}} \left(1 - \frac{\sqrt{k_{\frac{\pi}{2}\min}^2 - k_{0\min}^2}}{k_{\frac{\pi}{2}\min}} \cos\theta \right) < |k| \frac{k_{0\max}^2}{k_{\frac{\pi}{2}\max}} \left(1 - \frac{\sqrt{k_{\frac{\pi}{2}\max}^2 - k_{0\max}^2}}{k_{\frac{\pi}{2}\max}} \cos\theta \right) \\ 1 & |k| \frac{k_{0\max}^2}{k_{\frac{\pi}{2}\max}} \left(1 - \frac{\sqrt{k_{\frac{\pi}{2}\max}^2 - k_{0\max}^2}}{k_{\frac{\pi}{2}\max}} \cos\theta \right) \end{cases} \quad (4)$$

$$k = \begin{bmatrix} k_x \\ k_y \end{bmatrix}$$

Where the $k_{0\min}$ represents the minimum limit of the mask in 0° direction and so on.

here must be consistent.

$$\tilde{W}(k_x, k_y, f) = W(k_x, k_y, f) M_f(k_x, k_y) \quad (5)$$

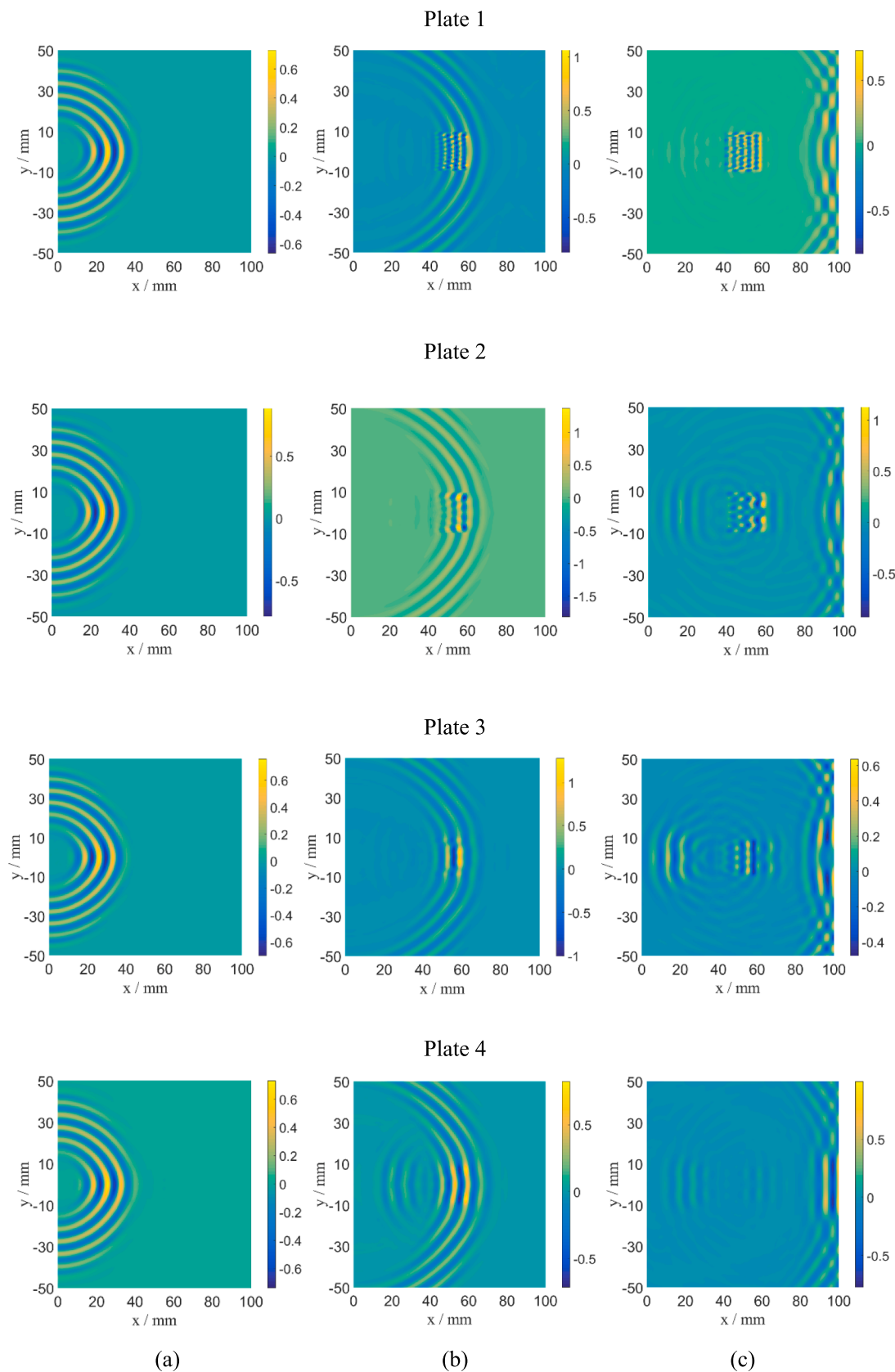


Fig. 7. Out-of-plane displacement of Lamb waves in the plates at (a)30 μ s; (b)50 μ s; (c)80.. μ s

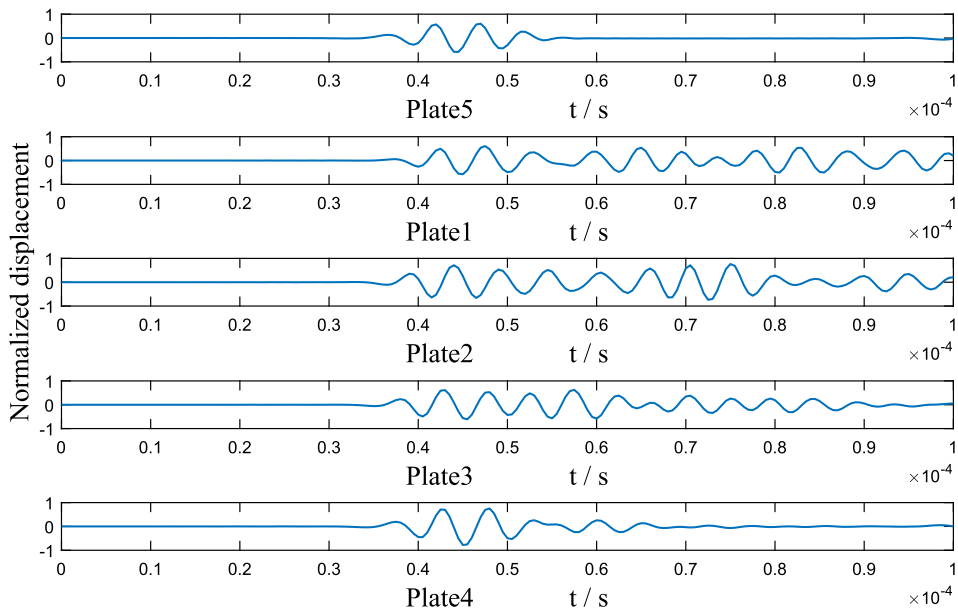


Fig. 8. Point (50, 0) mm vibrations in different plates.

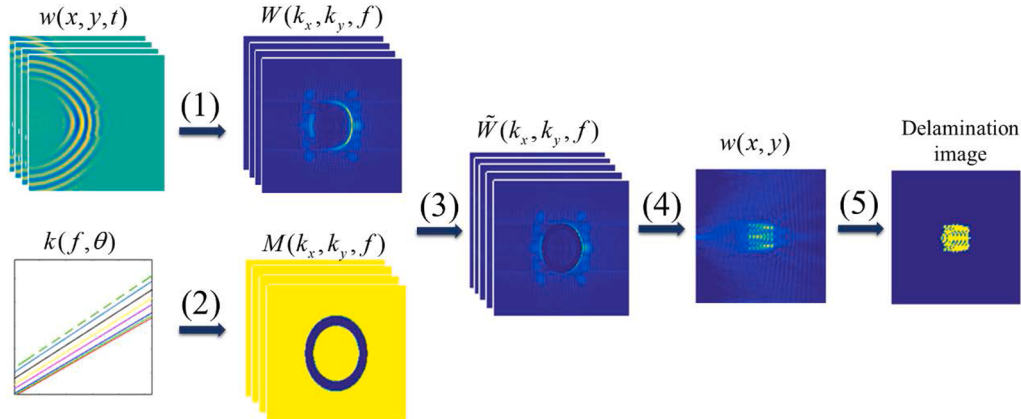


Fig. 9. Steps of SME delamination imaging method: (1) Transform time-domain wavefield to frequency domain through 3D-FFT; (2) Design the filter mask according to wavenumber dispersion curves; (3) Enhance the sensitive mode component; (4) Performing inverse Fourier transform; (5) Imaging using new modal components.

(4) Performing inverse Fourier transform

Perform inverse Fourier transform as Eq. (6) on the wavefield information after filtering out the originally existing A0 mode and return the enhanced-sensitive mode component to the space domain.

$$w(x, y, f) = F_{2D}^{-1} \{ \tilde{W}(k_x, k_y, f) \} \quad (6)$$

(5) Imaging using new modal components.

Follow Eq. (7) to average the new modal wavefield data at the above-selected frequencies and follow Eq. (8) to make thresholds (TH) according to experience.

$$\bar{w}(x, y) = \frac{1}{n} \sum_{f=f_1}^{f_n} w(x, y, f_n) \quad (7)$$

$$I(x, y) = \begin{cases} 1 & \bar{w}(x, y) > TH \\ 0 & \bar{w}(x, y) < TH \end{cases} \quad (8)$$

4. Results

4.1. Results of simulations

4.1.1. Results of SME imaging method

The SME imaging method in Section 3 was applied to the plate with delamination damage, and Fig. 10 presents the results. The signal-to-noise ratio (SNR) of simulation data is high, the TH was set to be 0.5. In fact, when the TH varies from 0.4 to 0.6, it doesn't make a different delamination image.

In the wavenumber-domain, the enhanced sensitive mode can be seen in. The enhanced sensitive mode shape is similar to an ellipse. The fewer layers contained by the top plate, the bigger value-sensitive mode has. Although the ellipse sizes are quite different in different plates, they can all provide correct delamination information. The sensitive mode is generated due to delamination, and in the time domain signal, it is aliased with other modes and difficult to distinguish. When the data is transformed into frequency-wavenumber-domain, it is clear and easy to pick up and enhance.

Table 3 shows the SME imaging results evaluation for this simulation section. Plate 1, plate 2, and plate 3 got satisfactory delamination

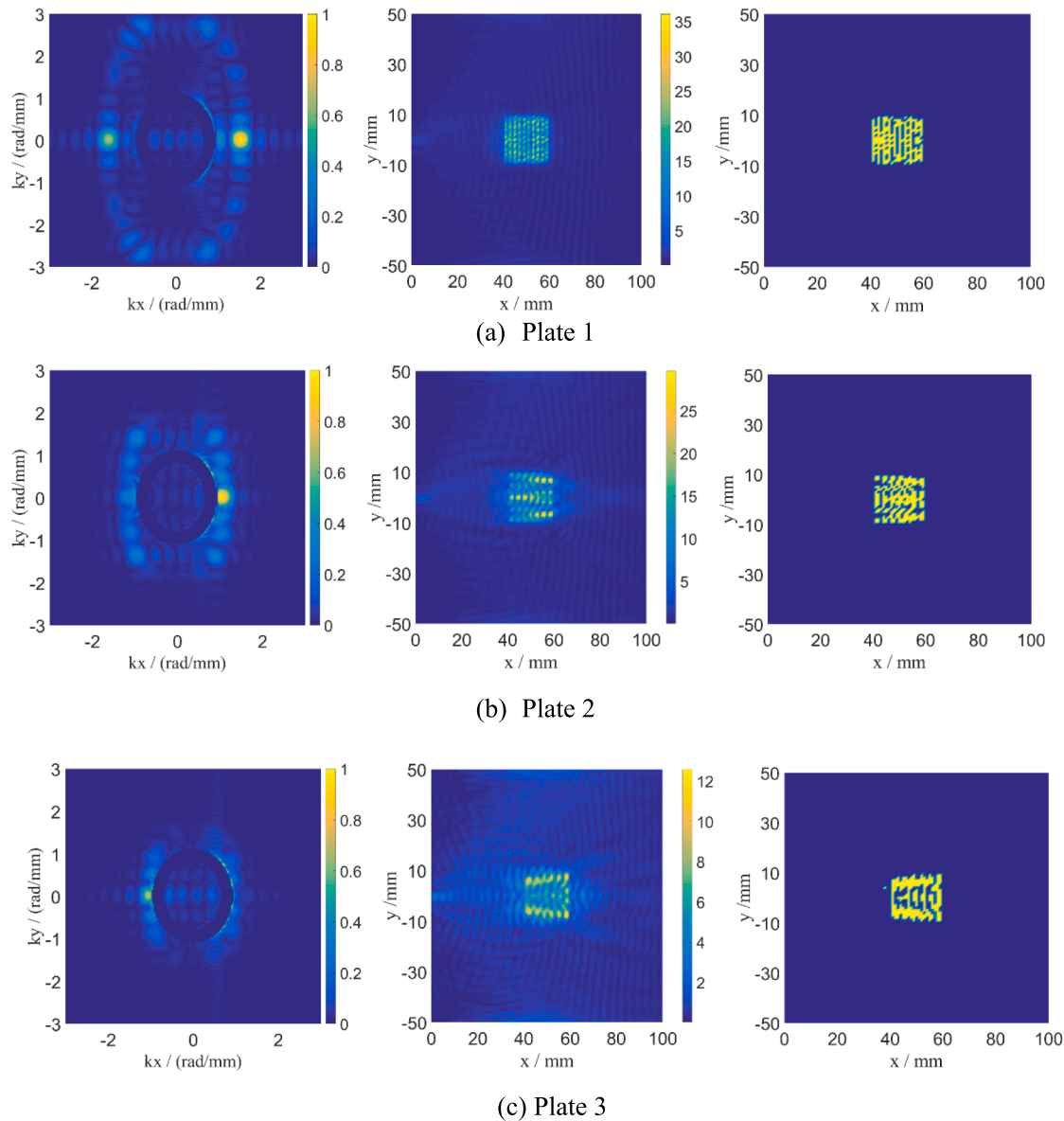


Fig. 10. SME imaging method process and results of simulations.

Table 3
SME imaging results evaluation for simulations.

	Deviation of center location(mm)	X-direction		Y-direction	
		Length (mm)	Deviation	Length (mm)	Deviation
Plate 1	0.5	18	10 %	20	0
Plate 2	0	18	10 %	18	10 %
Plate 3	0.5	19	5 %	18	10 %

images, the error is controlled within 10 %.

4.1.2. Sensitive mode analysis

According to the global matrix method mentioned in subsection 2.1, the dispersion curves of laminates with different layers of counts can be obtained. The wavenumber and the phase velocity have the relation $ck = \frac{f}{c_p}$. Thus, the wavenumber dispersion curves of different plies of

laminates can be easily calculated and shown in Fig. 11.

Since we chose 200 kHz as the center frequency of this research, we selected the wavenumber values at 200 kHz to compare with the wavenumber value of the sensitive mode.

It can be seen from Fig. 12 that the decreasing trend of theoretical and simulated wavenumber values is similar. Sensitive mode can be regarded as guided waves propagating in the upper sub-plate. And the wavenumber value of sensitive mode can be a basis for to detect the through-thickness location of the delamination. However, when number of plies is more than 5, the wavenumber value doesn't change much. Theoretically, the through-thickness location of the delamination damage can be obtained by the wavenumber value of the sensitive mode. In actual operation, only a rough estimate of the through-thickness location can be made.

4.2. Results of experiments

4.2.1. Experimental setup

The CFRP(T300) composite laminate plate measures $700 \times 300 \times 2$ mm, and is composed of 16 plies with layup $[+45/-45/0/0]_{2s}$, which has

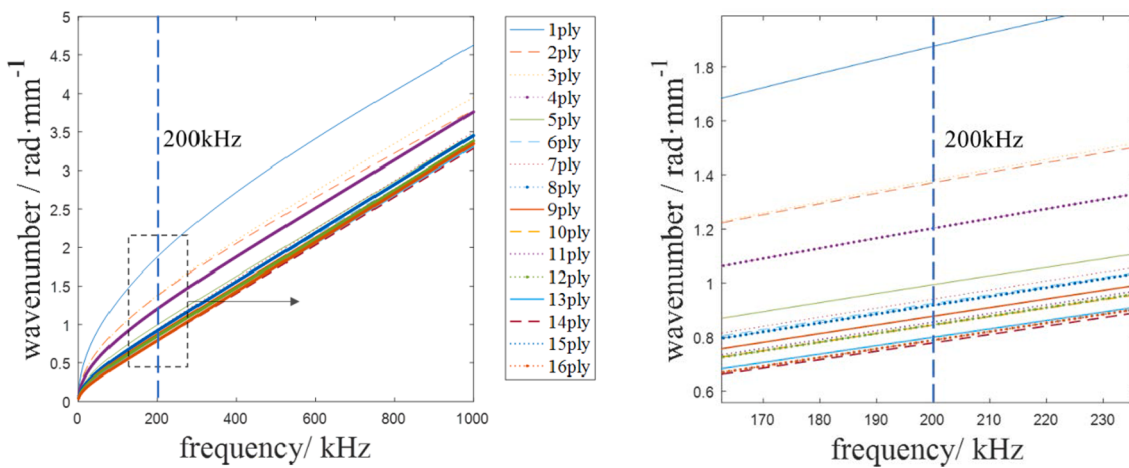


Fig. 11. Wavenumber dispersion curves of different plies of laminates.

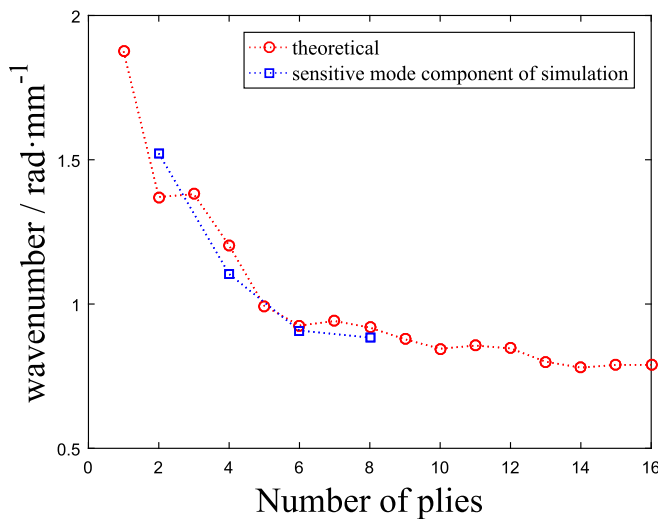


Fig. 12. Wavenumber of the sensitive mode component.

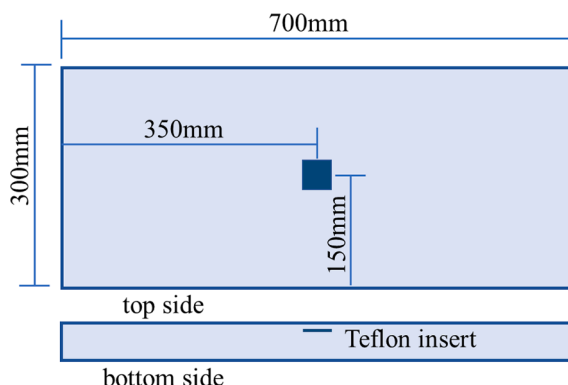


Fig. 13. Specimen with delamination scheme.

the same material characteristic as the numerical simulations. A 20×20 mm square Teflon insert was introduced to the sample during the manufacturing process between layers 4 and 5 to simulate delamination. The scheme of the sample with the delamination position is presented in Fig. 13.

In the tested specimen guided waves were excited by a round air-coupled ultrasonic transducer (Ultral Group NCG200-D25) with a

center frequency of 200 kHz and a bandwidth of 40 % of the center frequency. It emits ultrasonic waves to the surface of the investigated specimen at a specific angle fixed by a clamping device. The incident angle is calculated according to Snell's law, combined with the dispersion curve,

$$\sin(\theta_i) = \frac{v_{air}}{v_p} \quad (9)$$

Where v_{air} is the speed of sound in the air, and v_p is phase velocity of the guided waves. In this research the phase velocity of A0 mode at 200 kHz is 1592 m/s, and the best incident angle is $12^\circ 20'$.

The signal in a form of 5 sine cycles with 200 kHz frequency was generated by an arbitrary waveform generator (Siglent SDG 2042X) and amplified to 150 Vpp by a Linear Amplifier (Aigtek ATA-3080). Guided waves were measured by a scanning laser Doppler vibrometer (LDV) (Polytec PSV-500) as out-of-plane velocities in a regular grid of 47×47 points covering the top surface of the investigated specimen. The scheme of the experimental setup is presented in Fig. 14.

Measurements were synchronized with the excitation, and a 10 ms delay was set up to ensure the previously guided waves attenuate. In each measuring point, 5000 samples of time were registered with a 6.25 MHz sampling frequency, and the range of the band-pass filter is 100 ~ 300 kHz. Each point was measured 30 times and the averaged value was designed to improve signal quality.

4.2.2. Time-domain analysis

A few scanning points were selected along the x-axis, and the vibration signal was shown in Fig. 15. As the delamination damage is artificial and the location is clear, scanning points are selected in the damaged area. There are one main wave packet and several other wave packets travel along the x-axis. As time goes on, the wave after the fourth wave packet is hard to distinguish because of the dispersion effect and wave packet superposition. The group velocity of the first wave packet can be calculated as 1610.8 m/s which is approximate to the theoretical value in Fig. 2 (b) and the next three wave packets hold a group velocity of 431.9 m/s. The first wave packet is the direct A0 mode obviously, and the next three wave packets are new mode components appearing when the A0 mode spread to the delamination area. Our imaging method aims to enhance the new modal component and imaging with the enhanced components.

4.2.3. Result of SME imaging method

Limited by the number of sampling points, a Hanning window is added to the space domain and weaken Gibbs phenomenon. Fig. 16 presents the process of the SME imaging method. The original wavefield signal at $144 \mu\text{s}$ and the 3D Fourier transformed signal at 200 kHz are

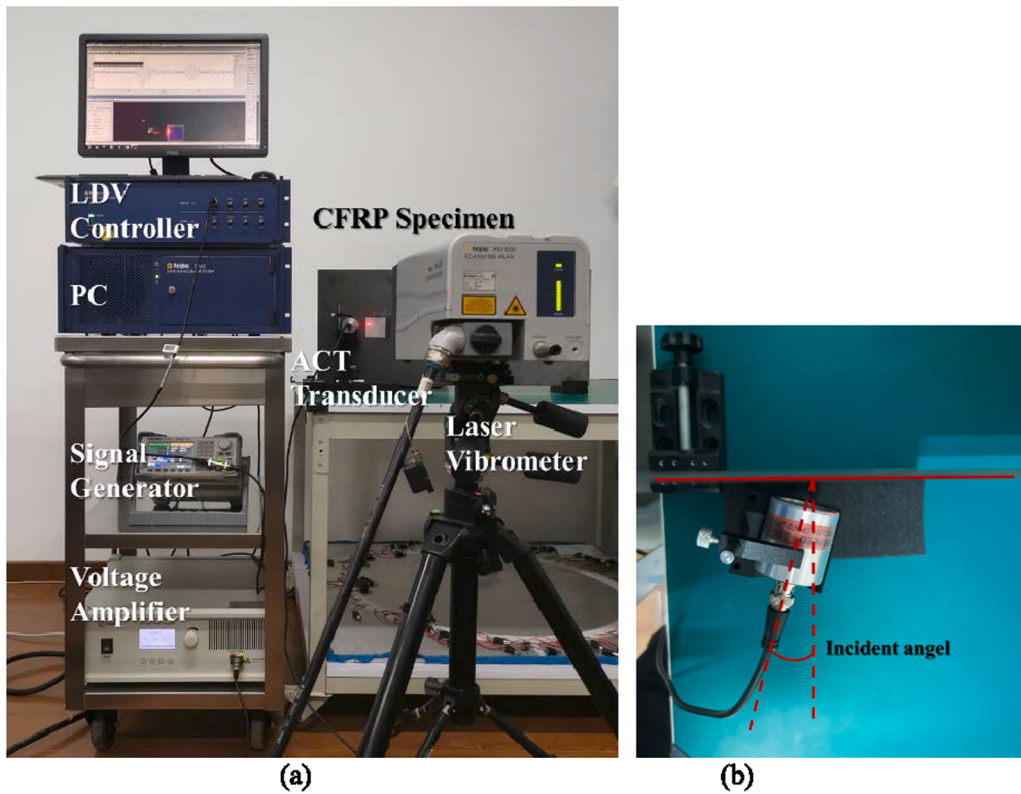


Fig. 14. Experimental setup: (a) overall set up; (b) incident angle set up.

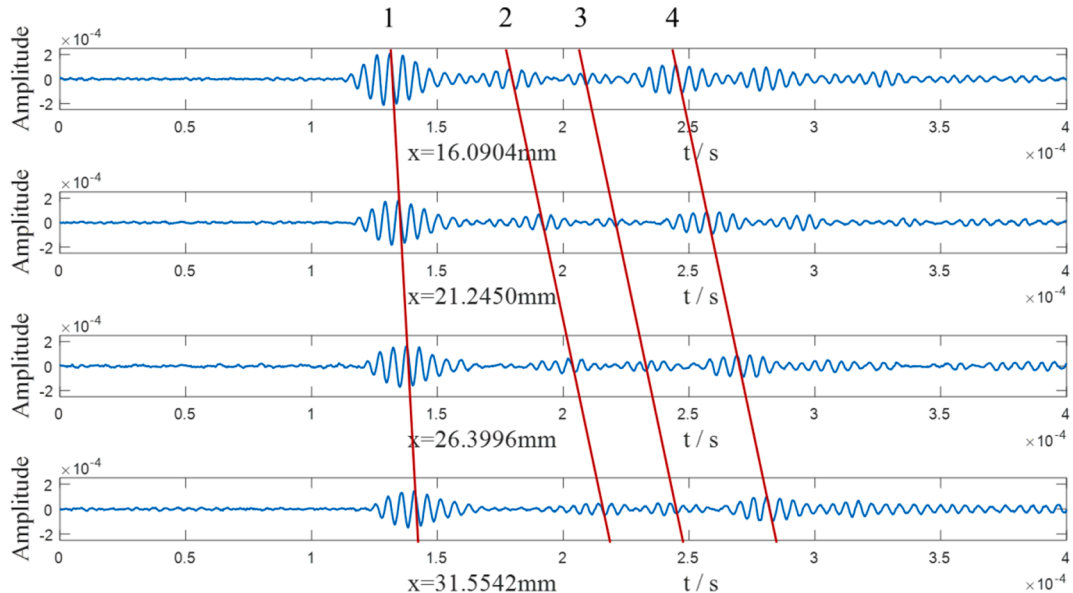


Fig. 15. Vibration signal of a few points.

shows in Fig. 16 (a) and (b). In the actual method process, several frequencies (170 kHz, 180 kHz, 190 kHz, 200 kHz, 210 kHz, 220 kHz, 230 kHz) were selected to contribute to damage detection. Fig. 17 shows the experimentally measured wavenumber values of the A0 modal wave and the theoretically calculated wavenumber values at different frequencies. And they matched well as shown in Fig. 17. Different filter masks were created according to the wavenumber values at different frequencies. Fig. 16 (c) exhibits an example of a filtered wavenumber-domain figure, and Fig. 16 (d) is the averaged inverse FT result of Fig. 16(c). The final delamination damage image is shown in Fig. 18 and the evaluation is

shown in Table 4. The red square is the actual delamination according to the machining drawing. According to experimental experience, the imaging threshold was selected as 0.38, and the coordinates in the figure are set by the LDV.

The experience detected the delamination damage successfully and imaged the delamination area. The longest lengths in the x and y directions were taken as the values for quantitative measurement of delamination damage. The center of the image is 2.50 mm far from the center of the prefabricated delamination and the deviation is 13.4 % in the x -direction and 10.6 % in the y -direction.

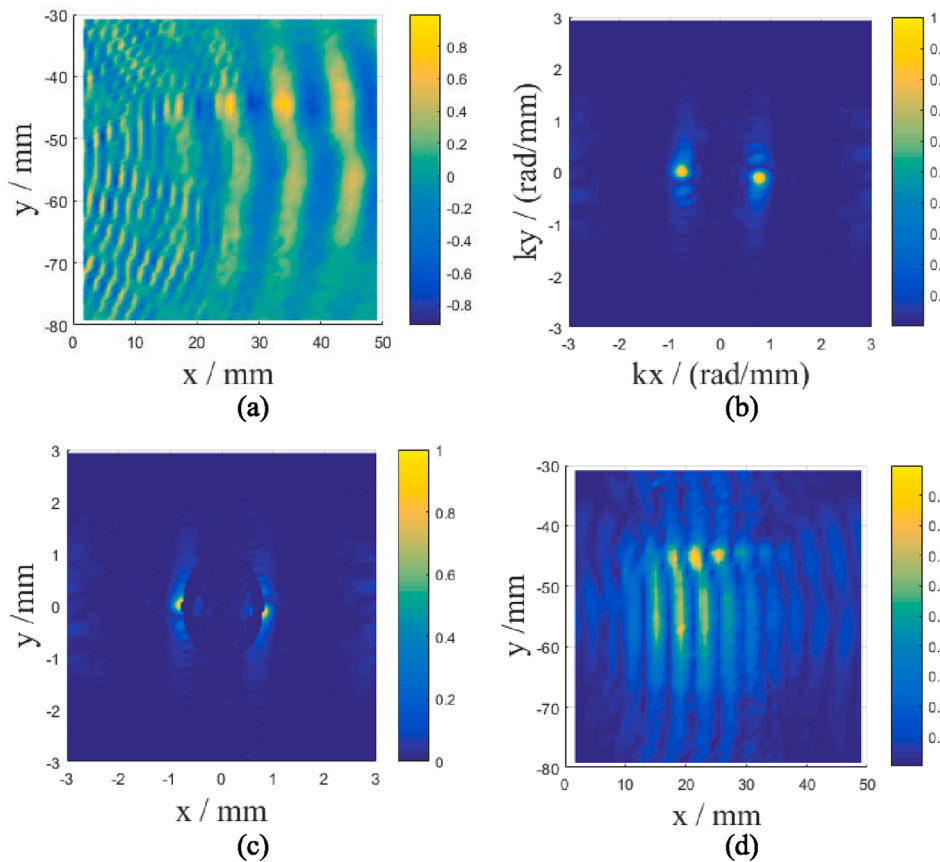


Fig. 16. Process of SME imaging method: (a) wavefield in time-domain; (b) wavenumber at 200 kHz; (c) filtered wavenumber at 200 kHz; (d) wavefield after inverse FT.

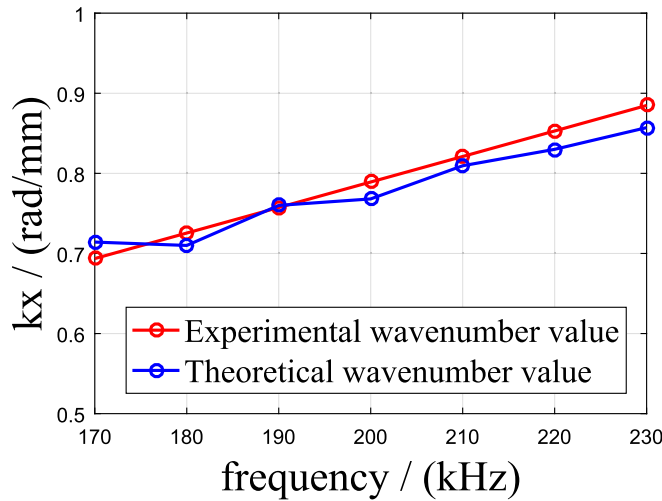


Fig. 17. Wavenumber value at various frequency.

As for through-thickness location of the delamination, it's difficult to get a trusted result. There are two reasons. First, the determination of the location depends on the wavenumber value of the sensitive mode. However, as shown in Fig. 11, when the number of upper sub-plate layers is more than 5, the wavenumber values are close to each other. A small deviation may cause quite different results. Second, there is a deviation between the guided wave modes in the experiment and the theoretical calculation, which leads to a error in determining the delamination position.

In this experiment, a non-focused air-coupled ultrasonic transducer

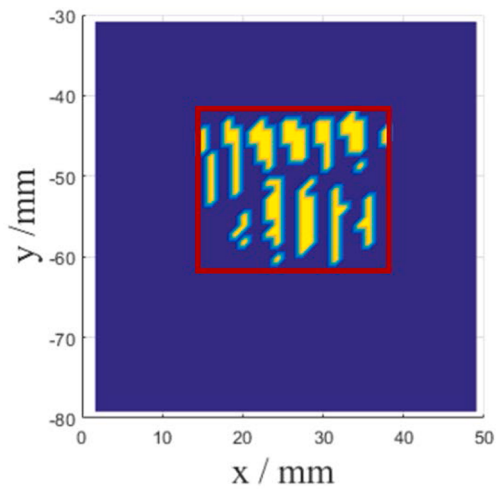


Fig. 18. Image of delamination damage.

Table 4
SME imaging result evaluation.

	Center location(mm)	Length in x-direction(mm)	Length in y-direction(mm)
Prefabrication information	(25, -55)	20.00	20.00
SME image of the delamination	(25.96, -52.67)	22.68	17.88
Deviation	2.50	13.4 %	10.6 %

was used to excite the signal, which set an incident angle and has good directivity. Therefore, the wavenumber-domain figure is an incomplete ellipse. While the ellipse annulus band stop filter applies to all direction excitation, which has a wide range of excitation form. Apart from air-coupled ultrasonic transducers, this method can also be applied to PZT transducers, Magnetostrictive sensors, and so on.

5. Conclusions

This present work aim to detect delamination damage in CFRP composite laminate plates.

Sensitive mode enhancement (SME) imaging method proposed in this paper based on sensitive mode component appearing at the delamination area. It takes full advantage of interactions between guided wave and delamination. SME imaging method deal with the wavefield in frequency-wavenumber-domain and the weak reflection characteristic was taken into consideration especially. It enhances the sensitive mode component appearing because of the delamination damage. The final delamination damage is obtained through energy intensity. The feasibility of the method is verified through numerical simulations, and the center position and size of the prefabricated delamination damage are detected through experiments with a non-contact air-coupled ultrasonic system. The experimental procedure detected the delamination damage successfully and imaged the delamination area.

In light of the obtained results, we can state that:

1. The SME imaging method is an effective method for delamination detection. It can obtain the morphology of the damage. The center of the image is 2.50 mm far from the center of the prefabricated delamination and the deviation is 13.4 % in the x-direction and 10.6 % in the y-direction.
2. At the delamination area, the guided waves propagate in the sub-plates separately. The mode components at this area are the basis of the detection.
3. According to the wavenumber value of the sensitive mode, we can roughly obtain the through-thickness location of delamination. But there are some difficulties when applying to experimental procedure.

Further research will be related to more accurate imaging results. Moreover, a problem of lifetime assessment of CFRP composite laminate structure will be investigated in further research. In addition, the accuracy of the through-thickness location of delamination is also worth improving if the actual engineering needs.

CRediT authorship contribution statement

Hui Zhang: Conceptualization, Methodology, Project administration. **Jing Sun:** Software, Validation, Writing – original draft. **Xiaobo Rui:** Investigation, Data curation, Writing – review & editing. **Si Liu:** Visualization.

Declaration of Competing Interest

The authors declare that they have no known competing financial interests or personal relationships that could have appeared to influence the work reported in this paper.

Data availability

Data will be made available on request.

Acknowledgement

This work is supported by National Nature Science Foundation of China (61771337, 62103297), and Project funded by China

Postdoctoral Science Foundation (2021 M700098).

References

- [1] Giurgiutiu V. Structural health monitoring (SHM) of aerospace composites [M]. Polymer composites in the aerospace industry. Elsevier 2020:491–558.
- [2] Zimmermann N, Wang PH. A review of failure modes and fracture analysis of aircraft composite materials [J]. Eng Fail Anal 2020;115:104692.
- [3] Baker AA. Composite materials for aircraft structures [M]. Reston: American Institute of Aeronautics and Astronautics; 2004.
- [4] Mousavi M, Gandomi AH. Wood hole-damage detection and classification via contact ultrasonic testing [J]. Construction Building Materials 2021;307:124999.
- [5] Taheri H, Hassen AA. Nondestructive ultrasonic inspection of composite materials: A comparative advantage of phased array ultrasonic [J]. Appl Sci 2019;9(8):1628.
- [6] Zhang H, Liu S, Rui X, et al. A skin-core debonding quantitative algorithm based on hexagonal units reconstruction for air-coupled ultrasonic C-scan images of honeycomb sandwich structure [J]. Appl Acoust 2022;198:108964.
- [7] Garcea S, Wang Y, Withers P. X-ray computed tomography of polymer composites [J]. Composites Science Technology 2018;156:305–19.
- [8] Wang Y, Burnett TL, Chai Y, et al. X-ray computed tomography study of kink bands in unidirectional composites [J]. Compos Struct 2017;160:917–24.
- [9] Bao Y, Wan T, Liu Z, et al. Integral equation fast solver with truncated and degenerated kernel for computing flaw signals in eddy current non-destructive testing [J]. NDT&E International 2021;124:102544.
- [10] E. Farag H, Toyserkani E, Khamese M B. Non-Destructive Testing Using Eddy Current Sensors for Defect Detection in Additively Manufactured Titanium and Stainless-Steel Parts [J]. Sensors, 2022, 22(14): 5440.
- [11] Tao N, Anisimov AG, Groves RM. FEM-assisted shearography with spatially modulated heating for non-destructive testing of thick composites with deep defects [J]. Compos Struct 2022;297:115980.
- [12] Chrysafi A, Athanasiopoulos N, Siakavellas N. Damage detection on composite materials with active thermography and digital image processing [J]. Int J Therm Sci 2017;116:242–53.
- [13] Hasiotis T, Badogiannis E, Tsouvalis NG. Application of ultrasonic C-scan techniques for tracing defects in laminated composite materials [J]. Mech Eng 2011;57(3):192–203.
- [14] Li H, Zhou Z. Detection and characterization of debonding defects in aeronautical honeycomb sandwich composites using noncontact air-coupled ultrasonic testing technique [J]. Appl Sci 2019;9(2):283.
- [15] Santos M, Santos J, Reis P, et al. Ultrasonic C-scan techniques for the evaluation of impact damage in CFRP [J]. Materials Testing 2021;63(2):131–7.
- [16] Tian Z, Yu L, Leckey C. Rapid guided wave delamination detection and quantification in composites using global-local sensing [J]. Smart Materials Structures 2016;25(8):085042.
- [17] Caminero M, García-Moreno I, Rodríguez G, et al. Internal damage evaluation of composite structures using phased array ultrasonic technique: Impact damage assessment in CFRP and 3D printed reinforced composites [J]. Compos B Eng 2019; 165:131–42.
- [18] Kažys R, Demčenko A, Žukauskas E, et al. Air-coupled ultrasonic investigation of multi-layered composite materials [J]. Ultrasonics 2006;44:819–22.
- [19] Mei H, James R, Haider MF, et al. Multimode guided wave detection for various composite damage types [J]. Appl Sci 2020;10(2):484.
- [20] Tian Z, Yu L, Leckey C. Delamination detection and quantification on laminated composite structures with Lamb waves and wavenumber analysis [J]. Journal of Intelligent Material Systems Structures 2015;26(13):1723–38.
- [21] Li J, Lu Y, Lee YF. Debonding detection in CFRP-reinforced steel structures using anti-symmetrical guided waves [J]. Compos Struct 2020;253:112813.
- [22] Jhang K-Y. Nonlinear ultrasonic techniques for nondestructive assessment of micro damage in material: a review [J]. International journal of precision engineering manufacturing 2009;10(1):123–35.
- [23] Pruell C, Kim J-Y, Qu J, et al. Evaluation of fatigue damage using nonlinear guided waves [J]. Smart Materials Structures 2009;18(3):035003.
- [24] Rekatsinas CS, Saravanos DA. A cubic spline layerwise time domain spectral FE for guided wave simulation in laminated composite plate structures with physically modeled active piezoelectric sensors [J]. International Journal of Solids Structures 2017;124:176–91.
- [25] Balasubramanian K, Sikdar S, Wandowski T, et al. Ultrasonic guided wave-based debond identification in a GFRP plate with L-stiffener [J]. Smart Materials 2021;31 (1):015023.
- [26] Williams W B, Michaels T E, Michaels J E. Application of wavefield imaging to characterize scattering from artificial and impact damage in composite laminate panels; proceedings of the AIP Conference Proceedings, F, 2018 [C]. AIP Publishing LLC.
- [27] Liu X, Bo L, Yang K, et al. Locating and imaging contact delamination based on chaotic detection of nonlinear Lamb waves [J]. Mechanical Systems Signal Processing 2018;109:58–73.
- [28] Rekatsinas C, Chrysochoidis N, Saravanos D. Investigation of critical delamination characteristics in composite plates combining cubic spline piezo-layerwise mechanics and time domain spectral finite elements [J]. Wave Motion 2021. 106 (102752).
- [29] Tian Z, Yu L. Lamb wave frequency-wavenumber analysis and decomposition [J]. Intelligent Material Systems Structures 2014;25(9):1107–23.
- [30] Radziński M, Kudela P, Marzani A, et al. Damage identification in various types of composite plates using guided waves excited by a piezoelectric transducer and measured by a laser vibrometer [J]. Sensors 2019;19(9):1958.

- [31] He J, Leckey CA, Leser PE, et al. Multi-mode reverse time migration damage imaging using ultrasonic guided waves [J]. *Ultrasonics* 2019;94:319–31.
- [32] Yelve NP, Mitra M, Mujumdar P. Detection of delamination in composite laminates using Lamb wave based nonlinear method [J]. *Compos Struct* 2017;159:257–66.
- [33] Mei H, Giurgiutiu V. Characterization of multilayer delaminations in composites using wavenumber analysis: numerical and experimental studies [J]. *Appl Sci* 2021;20(3):1004–29.
- [34] Kudela P, Radzieński M, Ostachowicz W. Identification of cracks in thin-walled structures by means of wavenumber filtering [J]. *Mechanical Systems Signal Processing* 2015;50:456–66.
- [35] Yu L, Tian Z, Leckey CA. Crack imaging and quantification in aluminum plates with guided wave wavenumber analysis methods [J]. *Ultrasonics* 2015;62:203–12.
- [36] Obenchain MB, Cesnik CE. Producing accurate wave propagation time histories using the global matrix method [J]. *Smart Mater Struct* 2013;22(12):125024.